GSC Biological and Pharmaceutical Sciences
eISSN: 2581-3250 CODEN (USA): GBPSC2
Cross Ref DOI: 10.30574/gscbps
Journal homepage: https://gsconlinepress.com/journals/gscbps/

(RESEARCH ARTICLE)

Check for updates

Videoing B and its Stereoisomers as Inhibitors of Nipah Virus- An *In-silico* Study of Structure-Based Virtual Screening and Comparative ADMET Profiling

Kulsoom Bano Z Sayed, Deepa N Rangadal and Shubhangi P Patil *

Department of Chemistry, The Institute of Science, 15, Madam Cama Road, Mantra Laya, Fort, Mumbai, Maharashtra 400032, India.

GSC Biological and Pharmaceutical Sciences, 2025, 33(01), 344-363

Publication history: Received on 06 September 2025; revised on 26 October 2025; accepted on 29 October 2025

Article DOI: https://doi.org/10.30574/gscbps.2025.33.1.0399

Abstract

Nipah virus (NiV) can cause a pandemic. Since there are no effective treatments available for NiV, the development of drugs requires immediate attention. In the context of drug discovery, natural products have emerged as a promising branch with tremendous scope. In this study, we screened 959 phytochemicals from 10 Indian medicinal plants using the IMPPAT database, PyRx, ProTox 3.0, SwissADME and AutoDock 4. Videoin B (L2) bypassed all 7 screening levels. Its stereoisomeric forms (1R,2R,4aS,6S,8aS)-2,5,5,8a-tetramethyl-5'-oxo-octahydro-2H-spiro[naphthalene-1,2'-oxolan]-6-yl acetate (L1) and (1S,2S,4aR,6R,8aR)-2,5,5,8a-tetramethyl-5'-oxo-octahydro-2H-spiro[naphthalene-1,2'-oxolan]-6-yl acetate (L3) were obtained from the LOTUS database. L1, L2 and L3 showed binding score of -6.7, -7.5 and -7.8 kcal/mol respectively, better than the standard- Ribavirin (L0) when docked with the attachment glycoprotein of NiV. The impact of stereoisomerism on inhibitory action, drug-like properties, ADMET profiles, and toxicology was thoroughly examined by using ADMETlab. Better docking scores, improved pharmacokinetics, medicinal properties, ADMET profiles and reduced toxicity concerns suggest that these three natural products- L1, L2 and L3 can be potent candidates for the novel drug discovery of Niv. Hence, this study is a step towards pandemic preparedness and aims to contribute to the drug development of deadly NiV.

Keywords: Nipah Virus; *In-Silico* Analysis; Structure-Based Virtual Screening; Stereoisomers; Docking; ADMET

* Corresponding author: Shubhangi P Patil

Graphical Abstract

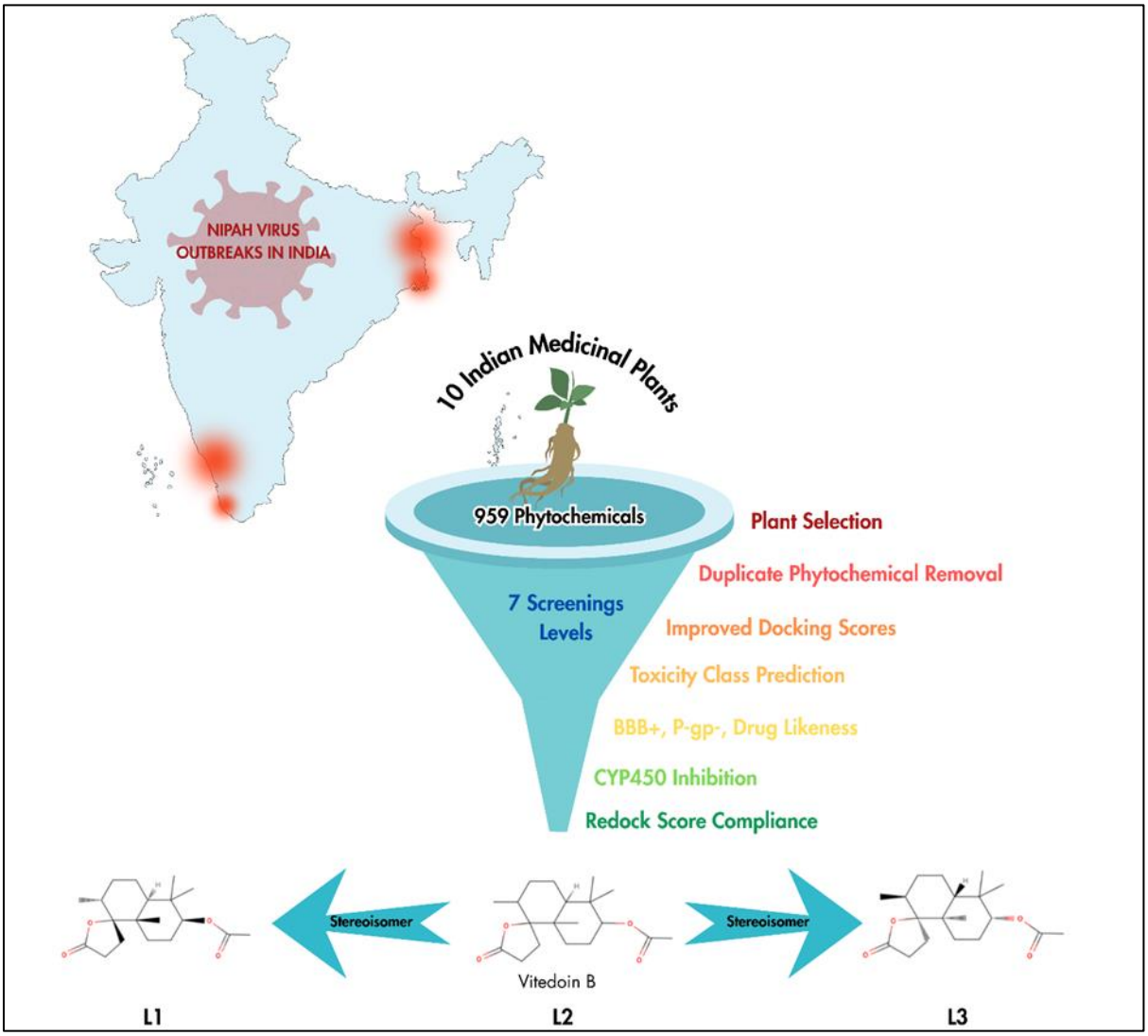

1. Introduction

Nipah virus (NiV) belongs to genus *henipavirus*, family Paramyxoviridae and order Mononegaviruses (1–4). It is a highly pathogenic, zoonotic virus (5). It is enveloped, has negative-sense single-stranded RNA and is considered a pathogen corresponding to biosafety level 4, hence needing utmost care in laboratory handling (2,6,7). Pteropid fruit bats, also called as flying foxes, are primarily the natural reservoir of NiV (2,6,8–12). Their excreta and saliva help in transmitting the virus and causing disease to secondary hosts/intermediate hosts (domestic animals like pigs, goats, horses, etc.), which in turn spread infection in humans when consumed (5,13). Humans and animals can develop the disease by eating bat-bitten dates or other fruits. The viral envelope has the attachment G and fusion F protein responsible for its entry into the host cell (11,14). Broad-spectrum antivirals like Ribavirin, Remdesivir and Flavipiravir are used in the treatment of NiV (3,4,15). NiV infections lead to inflammation of the brain, causing encephalitis and eventually death (2,15). Since it has high death rates, researchers are in desperate search of an effective medication, for which natural products can turn out to be a good option. In the context of drug discovery, this branch has limited exploration and tremendous scope. Direct lab exploration is immensely time and resource-consuming; hence, in-silico approaches are used to bridge this gap and save time and resources.

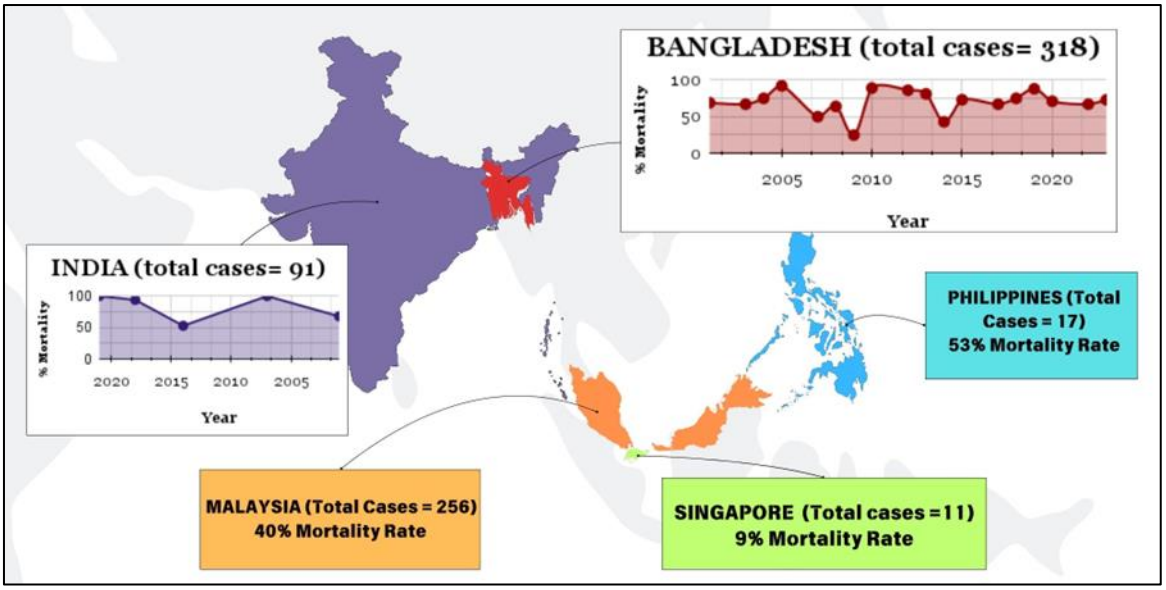

Figure 1 Global impact and percent mortality rate of Niv

Countries in which NiV spread has been reported are Malaysia, Singapore, Philippines, India and Bangladesh (16–18). Global impact has been shown in Fig. 1, which gives the mortality rate from year 1998 to 2023 for each country. The first outbreak was in Malaysia in 1998 with a 40% mortality rate, followed by Singapore in 1999 with a mortality rate as low as 9%. Similarly, there was only one outbreak in Philippines in 2014. Bangladesh had the maximum number of cases with a considerably high fatality rate, almost every year. India comes second in the list, but the outbreak was not observed regularly, as seen in the case of Bangladesh. In 2021, India had a 100% mortality rate. In India, the first outbreak was in Siliguri City (West Bengal) in 2001 (1,6). There are 2 strains of this virus- Bangladeshi and Malaysian, the former being more virulent than the latter because it shows human-to-human transmission and is circulated in India due to close geographical proximity. This virus is currently restricted to certain regions, but it is capable of causing a pandemic (2).

Natural products (NPs) and their derivatives show good results in clinical trials as effective drugs because they exhibit less toxicity as compared to synthetic drugs (19–21). Well-known anti-inflammatory drug acetylsalicylic acid, derived from *Salix alba* plant's active component, is one of the most successful drugs marketed (22,23). Another such example is *Colchicine* from *Colchicum autumnale*, used for gout and various other inflammatory diseases (22,24). For COVID-19, Virofree was reported to fight SARS-CoV-2 infection (22). Furthermore, NPs used for COVID-19, like *Myricetin* (25,26), *Punicalagin* (26,27), *Gallinamide A* (26,28), have been reported. Few studied phytochemicals exhibiting Anti-HIV activity are *Daphneodorins A & B* (26,29), *Kleinhospitine E* (26,30), *Beesioside* (26,31). Anticancer agents have been developed by the U.S. National Cancer Institute with the help of NPs (32). Whereas *Bifucatriol* (26,33), *Kakeromamide* (26,34), *Halymeniaol* (26,35) are Anti-malarial agents obtained from plants. A few more reported compounds are *Ubonodin* (36), *Santacruzamate A* (26,37), *Honaucin A* (26,38,39). Automation can extensively and rapidly screen vast chemical libraries virtually against biological targets, speed up the drug discovery procedures (22,39–42).

In the present research, we aim to identify potential inhibitors of the attachment-G protein of NiV by virtually screening 959 phytochemicals present in 10 Indian medicinal plants, namely Patala (*Stereospermum suaveolens*), Shalaparni (*Desmodium gangeticum*), Musta (*Cyperus rotundus*), Chirayata (*Swertia chirata*), Guduchi (*Tinospora cordifolia*), Bhunimba (*Andrographis paniculata*), Patha (*Cissampelos pareira*), Vasaka (*Justicia adhatoda*), Agnimantha (*Clerodendrum phlomidis*) and Nirgundi (*Vitex negundo*). Vitedoin B and its stereoisomeric forms- (1R,2R,4aS,6S,8aS)-2,5,5,8a-tetramethyl-5'-oxo-octahydro-2H-spiro[naphthalene-1,2'-oxolan]-6-yl acetate and (1S,2S,4aR,6R,8aR)-2,5,5,8a-tetramethyl-5'-oxo-octahydro-2H-spiro[naphthalene-1,2'-oxolan]-6-yl acetate were thoroughly studied to analyse the impact of stereoisomerism on inhibiting activity, binding affinity, pharmacokinetics, ADMET profiles and toxicology of all these NiV attachment glycoprotein-inhibiting molecules.

2. Methods

2.1. Protein structure retrieval, quality assessment and structural validation.

With careful consideration of various important parameters, the best structure of attachment glycoprotein of NiV came out to be 2VWD.

The structure of the attachment glycoprotein- G (2VWD) given in Fig. 2 was obtained from RCSB PDB (https://www.rcsb.org/) Protein Data Bank, which is a well-known database containing structures of different proteins in different forms (43–45). The structure was downloaded in PDB format, available amongst the various download options. The PDB DOI of the chosen protein is https://doi.org/10.2210/pdb2VWD/pdb. The 3D structure verification and quality assessment were done using the ERRAT score (46), Verify3D (https://www.doe-mbi.ucla.edu/verify3d/) (47) and Ramachandran plot from Discovery Studio Visualizer(48).

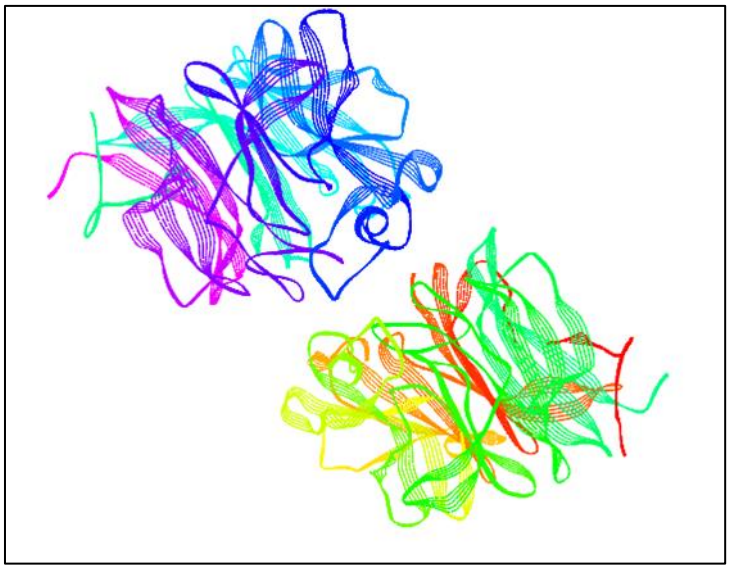

Figure 2 3D structure of the attachment glycoprotein (PDB ID: 2VWD) of Niva

2.2. Standard & Ligands structure retrieval.

Ribavirin, a broad-spectrum antiviral, was taken as the standard. Its structure was obtained from the PubChem database (https://PubChem.ncbi.nlm.nih.gov/) managed by the U.S National Institutes of Health (NIH) in SDF format, which was later converted to PDB and PDBQT format for docking. Structures of all phytochemicals present in 10 Indian medicinal plants were taken from the IMPPAT database (https://cb.imsc.res.in/imppat/). A similar structure search was done on PubChem. Stereoisomeric structures were obtained from the LOTUS database (https://lotus.naturalproducts.net/) (49). The molecular formula of all three ligands is $C_{19}H_{30}O_4$. Table 1 enlists the PubChem ID/ LOTUS ID, canonical smiles and the structures of the standard and ligand.

2.3. Docking

Initially, the protein preparation was done in UCSF ChimeraX 1.8 by removing all non-standard residues to remove the non-proteinous part and adding missing atoms, polar hydrogen and charges. Multiple docking for all phytochemicals with the druggable target (2VWD) was done in PyRx in 3 batches, having varied numbers of ligands. Later, L0, L1, L2 and L3 were docked with 2VWD in AutoDock 4 individually. After docking, binding affinities for the best binding pose of the ligand were tabulated in an Excel sheet. The output files generated contained the binding affinity of the top 9 poses, RMSD lower and upper bound and were saved as CSV files, which were further used for analysis.

2.4. ADMET Profiling

Initially, ProTox 3.0 (https://tox.charite.de/protox3/) software was used to know the toxicity classes of the phytochemicals and SwissADME (http://www.swissadme.ch/) was used to check the ADME profiles of the phytochemicals during the screening stage. L1, L2 and L3 showed better binding scores and ADMET profiles than the standard-L0. hence, detailed ADMET- absorption, distribution, metabolism, excretion and toxicity profiling of L1, L2 and

L3 was done in comparison with L0 with the help of ADMETlab (https://admetmesh.scbdd.com/). ADMETlab gave a detailed and complete analysis of all ADMET parameters(50).

Table 1 Ligands, their structures, IDs and canonical smiles

	Ligand	**Canonical Smiles**	**PubChem ID/ LOTUS ID**	**Structures**
L0	Ribavirin (Standard)	OC[C@H]1O[C@H]([C@@H]([C@@H]1O)O) n1cnc(n1) C(=O) N	37542	
L1	(1R,2R,4aS,6S,8aS)-2,5,5,8a-tetramethyl-5'-oxo-octahydro-2H-spiro[naphthalene-1,2'-oxolan]-6-yl acetate	CC(=O)O[C@H]1CC[C@@]2(C)[C@@H](CC[C@@H](C)[C@]23CCC(=O) O3) C1(C)C	Q105025374	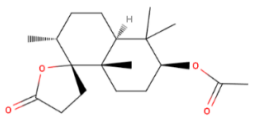
L2	2,5,5,8a-tetramethyl-5'-oxo-octahydro-2H-spiro[naphthalene-1,2'-oxolan]-6-yl acetate	CC(=O)OC1CCC2(C)C(CCC(C)C23CCC(=O) O3)C1(C)C	Q105025375	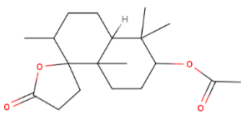
L3	(1S,2S,4aR,6R,8aR)-2,5,5,8a-tetramethyl-5'-oxo-octahydro-2H-spiro[naphthalene-1,2'-oxolan]-6-yl acetate	CC(=O)O[C@@H]1CC[C@]2(C)[C@H](CC[C@H](C)[C@@]23CCC(=O) O3) C1(C)C	Q105025376	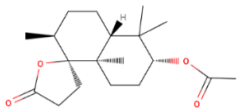

3. Results and Discussions

3.1. Structural validation and quality assessment of 2VWD

Ramachandran plot and Verify3D along with ERRAT score were used to assess the overall structural quality of the protein(51,52). Fig. 3 shows the Ramachandran plot with a high majority of protein residues in the most favoured region indicated by green, which is a very positive sign indicating that the protein's structure is energetically stable and well-defined. Very few points are in red, that is the disallowed region. Some of the residues in this region might be acceptable if they belong to flexible loops. The overall quality of the protein structure is good as suggested by the Ramachandran plot obtained from Discovery Studio Visualizer.

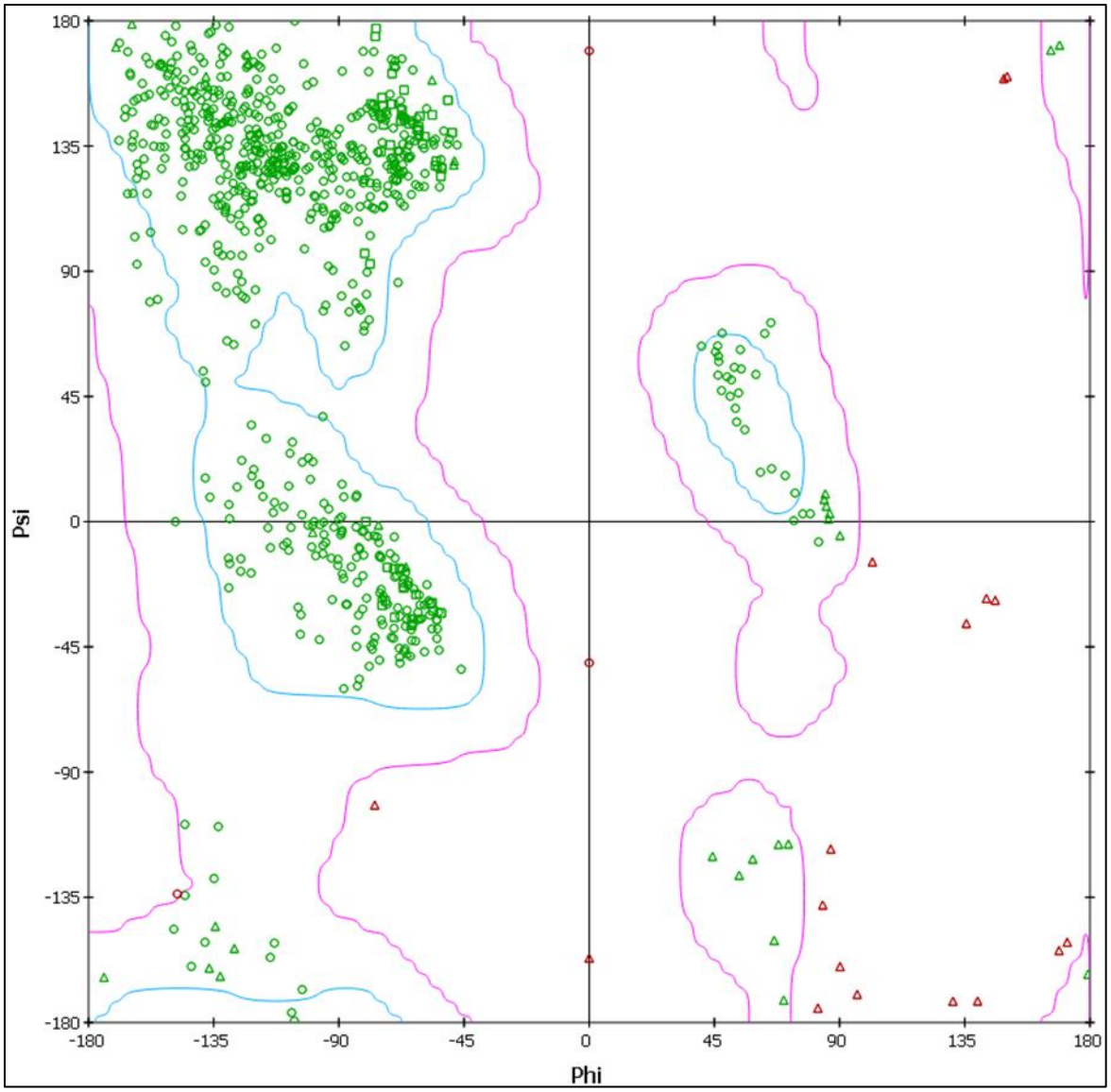

Figure 3 Ramachandran plot of the attachment glycoprotein of NiV (PDB ID- 2VWD)

Verify3D plot is used to check if the 3D structure of the protein complies with the 1D sequence and if the amino acid residues are in an energetically favoured environment(48,53). Positive values indicate a favourable environment, whereas negative values don't. A large majority of the scores for the residues are positive, as seen in Fig. 4, suggesting that the overall fold of the protein shows consistency with its 1D sequence, meaning they have a higher 3D-1D score. Although there are certain dips below zero, the overall quality of the protein structure based on sequence is good since 80.92% of the amino acids have the same 3D environment as suggested by the sequence, because they scored above 0.1, which is considered the threshold of acceptability. Thus, the verify3D plot also suggests that the protein structure meets the criteria for a good quality protein and hence, can be taken ahead for further studies. Lastly, on ERRAT, the protein structure was run and the overall quality factor of the protein structure was 93.4949 out of 100, indicating very high-quality protein.

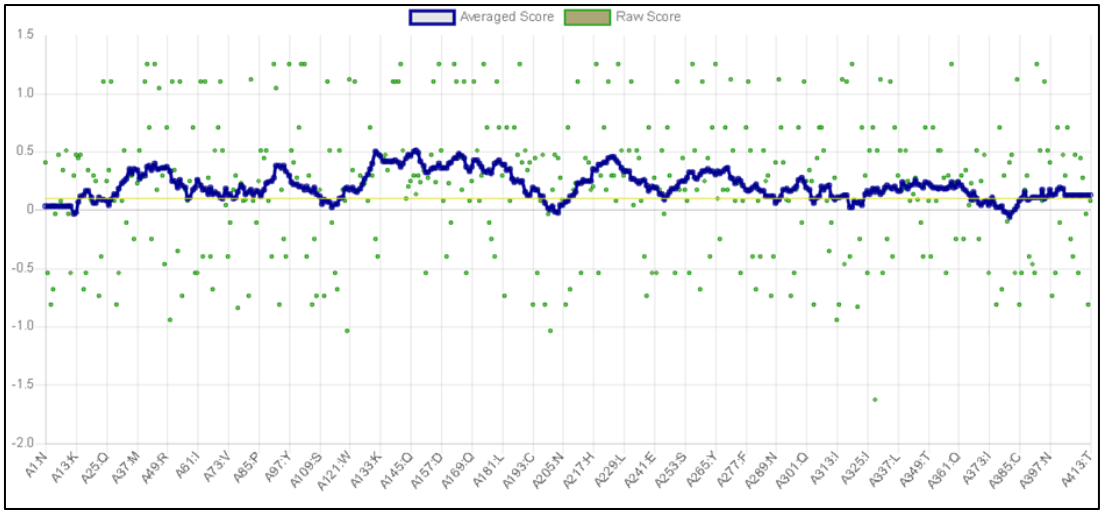

Figure 4 Verify3D plot for chain A and B of the attachment glycoprotein of NiV (PDB ID- 2VWD)

3.2. Virtual Screening

For 10 Indian medicinal plants, namely Patala (*Stereospermum suaveolens*), Shalaparni (*Desmodium gangeticum*), Musta (*Cyperus rotundus*), Chirayata (*Swertia chirata*), Guduchi (*Tinospora cordifolia*), Bhunimba (*Andrographis paniculata*), Patha (*Cissampelos pareira*), Vasaka (*Justicia adhatoda*), Agnimantha (*Clerodendrum phlomidis*) and Nirgundi (*Vitex negundo*), 959 phytochemicals were listed down from the IMPPAT database. Post elimination of duplicates, 470 remained. Docking of all these 470 phytochemicals and the standard was done with the Attachment Glycoprotein (2VWD) of Nipah virus. Results obtained from docking showed that out of these 470, 180 demonstrated better binding affinity than the standard-Ribavirin, which showed binding affinity = -6.6 kcal/mol. The toxicity classes of all these compounds were checked using ProTox-3.0 software. Compounds with toxicity classes 5 and 6 were screened out. 32 such compounds were found, out of which 27 were blood-brain barrier permeant, not a P-gap substrate and were drug-like. Only 2 did not inhibit the CYP450 enzymes. Lastly, only 1 compound, Videoin B (L2), complied with the original docking score on redocking individually, while the other did not. These 7 levels of screening are shown in Fig. 5. Hence, for Vitedoin B similar structure search was done with the help of PubChem and LOTUS databases, resulting in the selection of L1 and L3 as 2 non-planar stereoisomers of L2

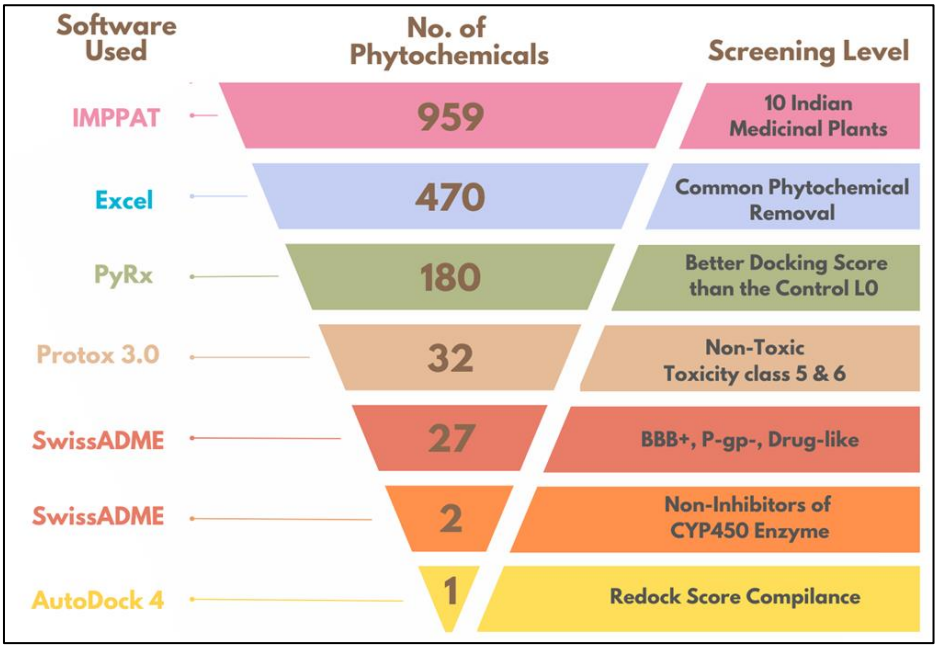

Figure 5 Various stages of Virtual Screening for Niv Lead Compound discovery

3.3. Docking results analysis

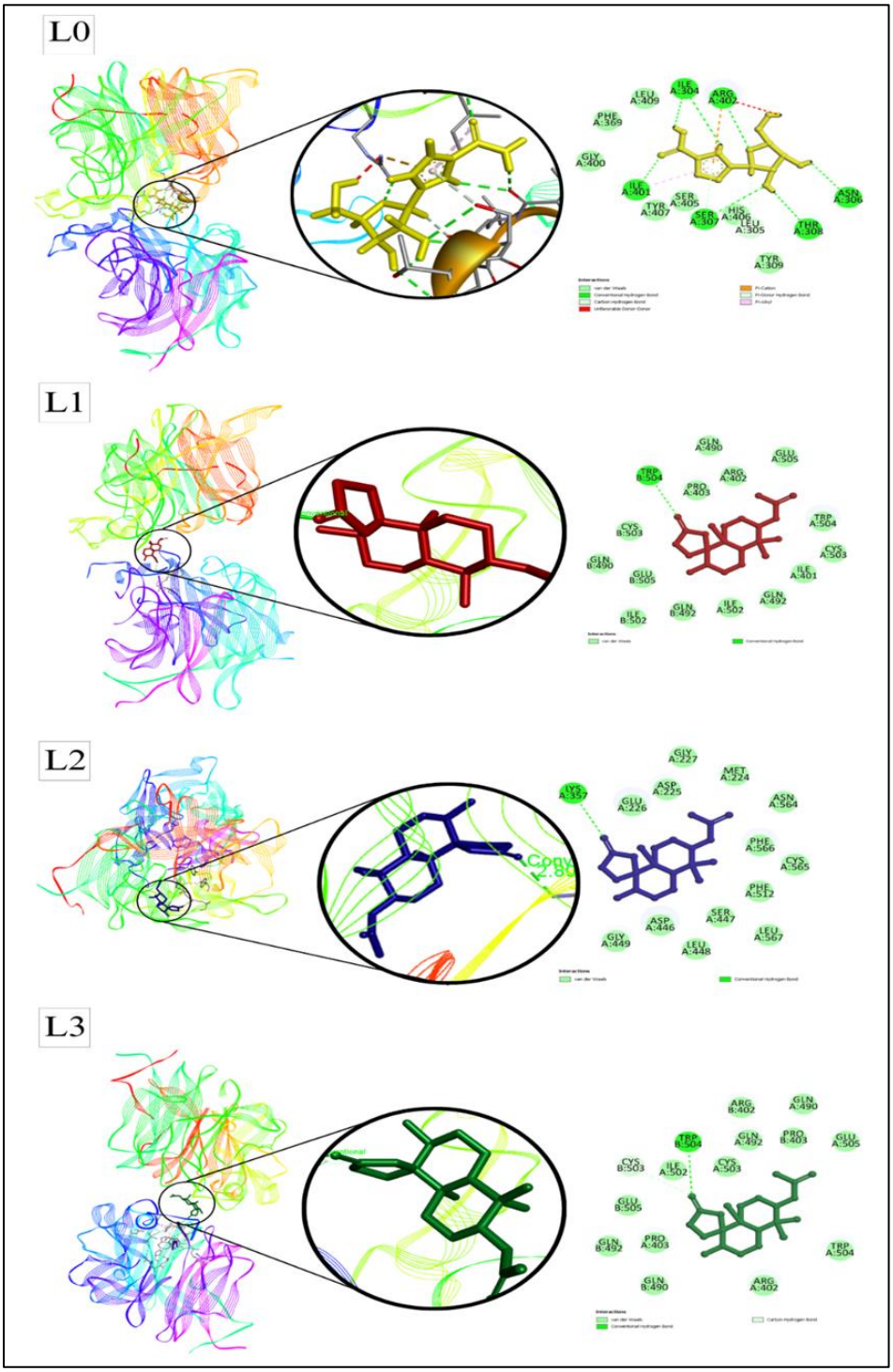

Figure 6 Best docked posed of L0, L1, L2 and L3 with protein 2VWD

3.3.1. Quantitative and comparative data analysis of binding affinities

Table 2 enlists the binding score, type of interactions between the ligand and the interacting amino acid residues and the binding site in which L0, L1, L2 and L3 are present. Fig. 6 shows the ligands bound in the binding pockets of the protein-2VWD, an enlarged view of the binding site and the 2D diagram showing different interactions present in the protein-ligand complex formation. L0 has a binding affinity of - 6.6 kcal/mol. L1 has a binding affinity - 6.7 kcal/mol. There is a difference of -0.1 units in the binding affinities of L0 and L1. L2 and L3 show significantly higher negative values of binding affinity than L0. L2 exhibits -7.5 and L3 shows -7.8 kcal/mol.

Table 2 Binding affinities, interaction types and binding site coordinates for protein in complexation with L0, L1, L2 and L3

Protein complexed with	Binding affinity (in kcal/mol)	Type of interactions	Binding site coordinates (x, y, z)
L0	-6.6	Unfavourable donor-donor Van der Waals Conventional hydrogen Carbon hydrogen Pi-cation Pi-donor hydrogen Pi-alkyl	-47.006413, -9.721968, -24.949323
L1	-6.7	Van der Waals Conventional hydrogen	-42.043783, -1.941174, -16.125174
L2	-7.5	Van der Waals Conventional hydrogen	-14.592783, -29.771478, -25.868087
L3	-7.8	Van der Waals Conventional hydrogen Carbon hydrogen	-41.927783, -1.905391, -16.008435

3.3.2. Structural differences and their impact

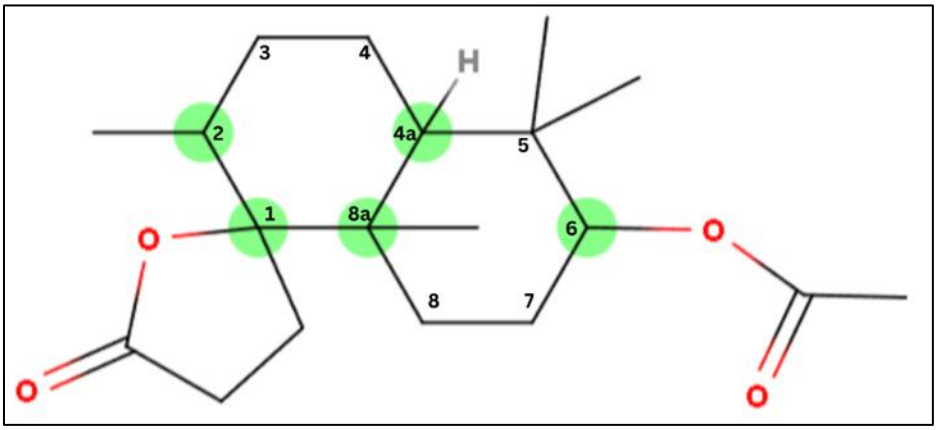

Figure 7 Common 2D diagram for L1, L2 and L3 with stereocenters

Three important key parameters affecting the binding affinity are planarity, stereochemistry and binding site coordinates. As seen in Table 2, L1, L2 and L3 share the same molecular formula $C_{19}H_{30}O_4$ and the same atom connectivity, but they have different spatial arrangements. Since all stereoisomers have different 3D diagrams but share the same 2D diagram, in Fig. 7, the Common 2D diagram for L1, L2, and L3 has been given with their stereocenters highlighted in green. There are 5 stereocenters for L1, L2 and L3 as mentioned in Table 3 and seen in Fig. 7. In L2, all the groups at the stereocenters lie in the plane of the paper, hence it demonstrates a planar structure, limiting its interactions to chain A of 2VWD. The 5 stereocenters in L1, L2, and L3 are C-1, C-2, C-4a, C-6 and C-8a where C1 is the spiro carbon atom connecting the naphthalene ring to the oxolan ring; C2 is the carbon atom bearing the methyl group on the naphthalene ring; C4a is the bridgehead carbon atom present between the two rings of the naphthalene; C6 bears the acetate group on the naphthalene ring and C8a again is the bridgehead carbon but it bears the methyl group on the naphthalene ring. For L1, stereochemistry is 1R,2R,4aS,6S,8aS as indicated by the name of the compound in Table 1. If 1R becomes 1S, 2R becomes 2S, 4aS becomes 4aR, 6S becomes 6R and 8aS becomes 8aR, that is, if the stereochemistry at the stereocenters of L1 is inverted, the resulting compound would be L3. Therefore, L1 and L3 are non-planar

structures, due to which they can access a binding site that is present between chain A and chain B. Thus, differences in the planarity directly influence the interaction profiles and the available binding pockets. Changing the stereochemistry of specific groups causes a difference of -1.1 units in the docking score, which highlights the sensitivity of binding affinity to minor stereochemical changes. The binding site coordinates for L1 and L3 are proximate. However, they still differ due to their distinct 3D conformation. This enables L1 and L3 to interact with different amino acid residues in chains A and B. Changes in stereochemistry alter the ability of the ligands to interact with the same set of residues, thus affecting binding affinity.

3.3.3. Correlation between interactions and the binding affinity

Conventional hydrogen bonds are important for improving the binding score. All three stereoisomers L1, L2 and L3 exhibit at least one conventional hydrogen bonding, due to which they have improved docking scores compared to L0, which displays an unfavorable interaction.

L3 has a unique feature compared to its other stereoisomers; it has an additional carbon-hydrogen bond present and hence has the best docking score. Carbon-hydrogen bond is a significant score-enhancing interaction. This additional feature enhances the docking score and makes L3 the most potent binder, having the highest negative value of binding affinity. Van der Waals interactions are present in all four ligands L0, L1, L2 and L3

L1 shows 14 Van der Waals interactions. L2 and L3 show 13 interactions. Although these interactions contribute less significantly to the docking score, the combined effect of numerous such interactions shows a significant impact in a positive manner. Hence, all the stereoisomers present better scores than the standard.

3.4. ADMET predictions

Table 3 ADMET predictions of L0, L1, L2 and L3

PARAMETERS UNDER EVALUATION		**LIGANDS**			
		L0	L1	L2	L3
Physicochemical properties	Molecular weight	244.08	322.21	32.21	32.21
	nHA	9	4	4	4
	nHD	5	0	0	0
	nRot	3	2	2	2
	nRing	2	3	3	3
	nHet	9	4	4	4
	fChar	0	0	0	0
	nRig	11	18	18	18
	Flexibility	0.273	0.111	0.111	0.111
	Stereocenters	4	5	5	5
	TPSA	**143.72**	52.6	52.6	52.6
Medicinal chemistry	QED	0.443	0.688	0.688	0.688
	SAScore	3.869	4.564	4.564	4.564
	Fsp3	0.625	0.895	0.895	0.895
	NPscore	0.691	3.128	3.128	3.128
	Lipinski rule	Accepted	Accepted	Accepted	Accepted
	GSK rule	Accepted	Accepted	Accepted	Accepted
	Golden triangle	Accepted	Accepted	Accepted	Accepted
	Colloidal aggregations	0.058	0.536	0.104	0.576

	Ghose rule	**No**	Yes	Yes	Yes
	Veber rule	**No**	Yes	Yes	Yes
	Egan rule	**No**	Yes	Yes	Yes
	Muegge rule	**No**	Yes	Yes	Yes
Absorption	Caco-2 Permeability update	-5.656	-4.696	-4.776	-4.784
	Pgp substrate	**0.675**	0.0	0.0	0.0
Distribution	PPB	15.11%	68.01%	86.92%	92.36%
	VDss	22.122	0.618	0.954	1.51
	BBB penetration	**No**	Yes	Yes	Yes
	Fu	83.61%	32.28%	17.26%	15.13%
Metabolism	CYP450	None	None	None	None
	GI absorption	**Low**	High	High	High
Excretion	CLplasma	4.206	6.367	4.444	7.947
	T1/2	0.721	0.263	0.232	0.166
Toxicity	Neurotoxicity	0.554	0.097	0.607	0.33
	Ototoxicity	**0.897**	0.175	0.43	0.281
	Hematotoxicity	**0.647**	0.524	0.254	0.389
	Nephrotoxicity	0.58	0.755	0.339	0.409
	Genotoxicity	**0.996**	0.476	0.019	0.752
	Immunotoxicity	0.069	0.026	0.047	0.051
	A549 cytotoxicity	0.021	0.115	0.086	0.121
	hERG blockers	0.018	0.049	0.036	0.014
	Hepatotoxicity	**0.777**	0.548	0.424	0.566
	DILI	**0.983**	0.558	0.475	0.344
	AMES toxicity	**0.806**	0.523	0.254	0.516
	Rat oral acute toxicity	0.01	0.109	0.098	0.053
	Carcinogenicity	0.183	0.305	0.07	0.041
	Eye irritation	0.134	0.984	0.558	0.043
	Respiratory toxicity	0.017	0.953	0.863	0.406
	Acute toxicity rule	0 alerts	0 alerts	0 alerts	0 alerts
	Genotoxic Carcinogenicity Rule	0 alerts	0 alerts	0 alerts	0 alerts
	NonGenotoxic Carcinogenicity Rule	0 alerts	0 alerts	0 alerts	0 alerts
	Skin Sensitization Rule	0 alerts	0 alerts	0 alerts	0 alerts
	Aquatic Toxicity Rule	0 alerts	2 alerts	2 alerts	2 alerts
	NonBiodegradable Rule	**1 alert**	0 alerts	0 alerts	0 alerts
	SureChEMBL Rule	0 alerts	0 alerts	0 alerts	0 alerts

Table 3 gives us detailed information about the physicochemical properties, medicinal chemistry and ADMET parameters for thorough theoretical evaluation.

3.4.1. Physicochemical property

Physicochemical properties are physical and chemical properties of a substance describing how it might behave based on its structure and composition (54–59). The physicochemical properties of all the stereoisomers are the same, but they differ from those of the standard. L0 is more polar than needed. For L1, L2 and L3. Molecular weight should range between 100 to 600, based on the drug-like soft rule (60). Similarly, the number of hydrogen bond acceptors should be between 0 to 12, and the number of hydrogen bond donors should be between 0 to 7. These are also based on drug-like soft rules. The number of rotatable bonds should be in the range 0 to 11. A molecule can have a maximum of six rings. optimal formal charge ranges between -4 to +4. The number of heteroatoms can be a minimum of 1 and a maximum of 15. The maximum number of rigid bonds can be 30. Flexibility is the ratio of the number of rotatable bonds divided by the number of rigid bonds. The number of stereo centres should be equal to or less than 2, which is based on the lead-like rules. Polar fragments contribute to the surface area; the sum of the contributions of all polar fragments is known as the topological polar surface area. Its optimal range is 0 to 140.

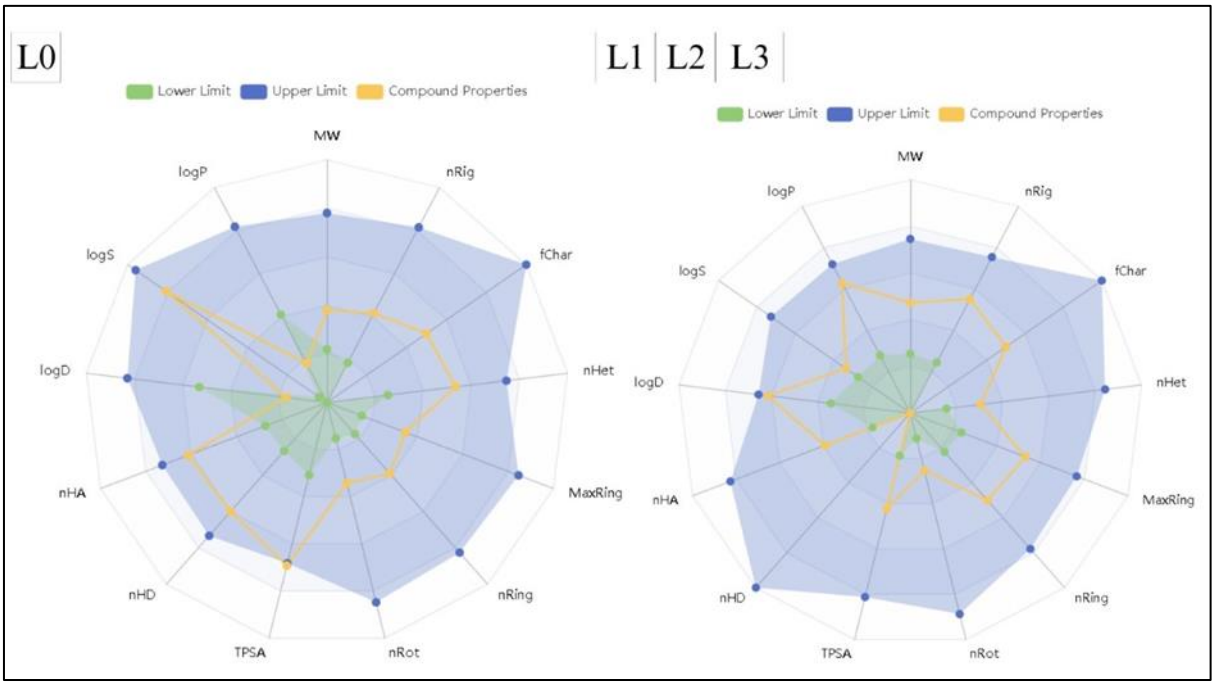

Figure 8 Spider web diagram for physicochemical properties with upper and lower limit

The spider web diagram in Fig. 8 for L0 highlights the values for physicochemical properties in and out of the ranges. The lower limit is marked by green, and the upper limit is marked by blue. The compound's properties are marked in yellow. The three stereoisomers in the spider web diagram are seen to lie in the optimal ranges. Despite different spatial arrangements, L1, L2 and L3 exhibit identical values. LogP and LogD values for L0 are less than the lower limit, and TPSA exceeds the upper limit. LogD is LogP but a pH-dependent version of the same. If LogP and LogD are lower, it means that the drug molecule is less lipophilic and more hydrophilic. Less lipophilic molecules are unable to cross a lipid-rich barrier like the BBB. It also indicates that the L0 has poor absorption in the GI tract because of its inability to pass through intestinal linings composed of lipid membranes. Such hydrophilic molecules will be excreted from the body very quickly. Distribution in tissues rich in lipid is also significantly hindered because of low absorption. TPSA higher than the desired value indicates increased polarity, limiting the ability to pass through the BBB, a lipid-rich membrane, as stated earlier. Poor oral bioavailability is a result of hindered ability to cross the intestinal lipid made molecules. Hence, the L0 is not likely to reach the bloodstream. This raises significant concerns about the absorption, distribution and overall potency and efficacy of L0.

3.4.2. Medicinal Chemistry

QED (Quantitative Estimate of Drug-likeness) calculates 8 drug-like parameters and measures drug-likeness (61,62). For all the stereoisomers, the QED score is the same and lies in an excellent range. Synthetic accessibility score should

be between 1-10 for all molecules, 10 being the toughest to synthesize. All SA Scores are in the acceptable range. The fraction of sp3 carbon is used to find out how three-dimensional the molecule is. Generally, a higher value is considered better and means that there are more sp3 hybridized carbons. All stereoisomers have a higher value than L0. NP score should be in the range -5 to +5. A higher score indicates a higher probability of being a natural product. The NP scores indicate that all stereoisomers are natural products, while the standard is not. The Lipinski rule of 5 is followed by all the ligands. Compounds satisfying the GSK rule and the golden triangle rule are predicted to have a more favorable ADMET profile. All stereoisomers are seen to follow the commonly employed rules like Ghose, Veber, Egan and Muegge, but L0 does not adhere to these rules. This is an indication of good oral absorption, reasonable bioavailability and fewer ADME issues. Formation of colloidal aggregates is not desirable because it prevents the molecule from binding to the surface of the desired disease-causing protein. L0 has the least possibility, and L2 has an extremely small score for the formation of aggregate colloidal amongst all stereoisomers.

3.4.3. Absorption

Absorption measures how a drug travels from the site of administration to the site of action (63). A drug which is administered orally has to pass through the intestinal cells either by passive diffusion or active transport processes or carrier-mediated uptake (64). The human colon adenocarcinoma cell lines are studied to estimate the permeability of the drug in in-vivo analysis. A value above 5.15 is generally considered good. The values in the table indicate that the standard is a PGP substrate; that is, it will be pumped out of the cell limiting its efficacy.

3.4.4. Distribution

Drug distribution refers to how drugs move through various tissues of the body and the amount of drugs in the tissues (65). Plasma protein binding (PPB) directly affects oral bioavailability because if the drug binds to the plasma protein, its concentration in the free state is at stake, hence, its value should be less than 90% (66). The standard-L0 has the lowest PPB percent. L1 and L2 show plasma binding less than 90% conversely, L3 shows 92.36% PPB. Thus, due to a change in the stereochemistry, there is a severe impact on the therapeutic index. L3 has the least therapeutic index due to the highest plasma protein binding, and L1 has a better therapeutic index than L2. VDss is the volume of distribution at steady state, it is a measure of effective distribution of the drug molecule throughout the body (67,68). A lower value is considered favourable because a higher value indicates the probability of unpredictable distribution. The standard comparatively has the highest value. The values are very low for the stereoisomers. L0 is not permeable through the blood-brain-barrier; on the other hand, L1, L2 and L3 are, which is also seen in the BoiledEGG Model given in Fig. 9. Fraction unbound plasma percent (Fu%) should be higher, indicating a high concentration of drug in the free state available for binding with the desired protein site (69,70). The standard shows a higher Fu%, whereas the three stereoisomers exhibit a low percentage.

3.4.5. Metabolism

Drug metabolism measures the drug's action intensity and how it is broken down by the enzymes. CYP450 enzymes are a set of enzymes present in the liver responsible for breaking down drug molecules. Their activity should not be slowed down or inhibited (71–75). None of the molecules is known to inhibit these enzymes. GI Absorption of L0 is low, which means it will have poor bioavailability. L1, L2, and L3 show high absorption in the GI track, which is clearly seen in Fig. 9.

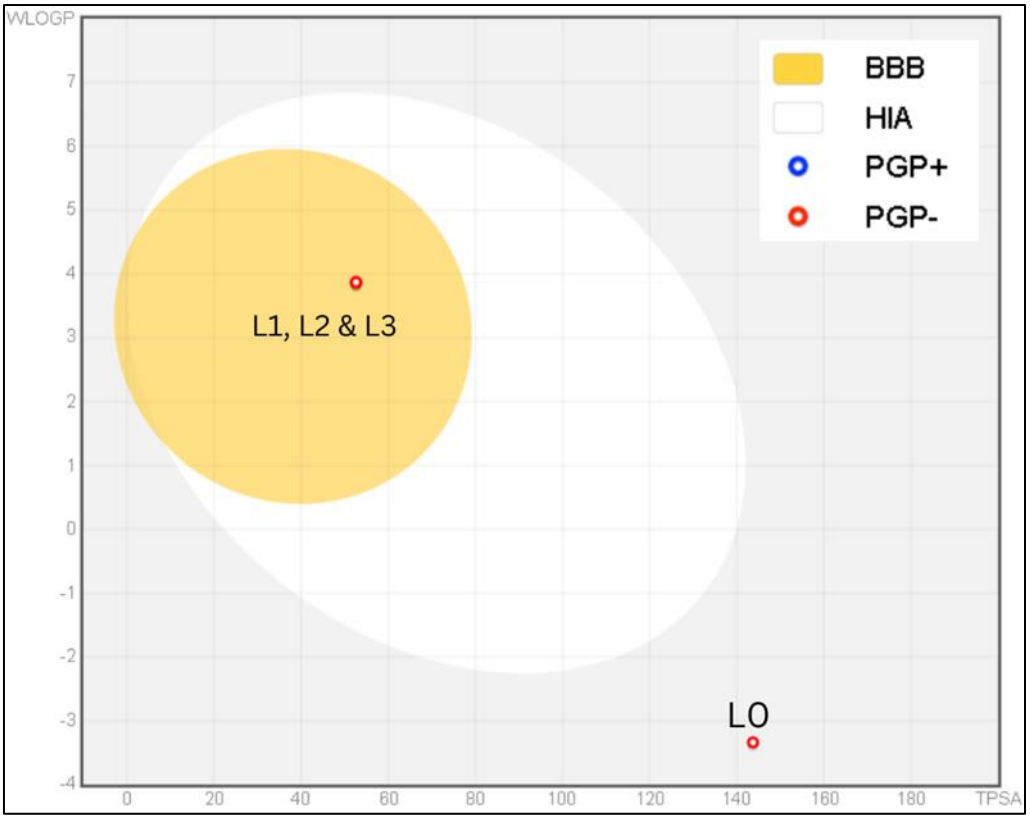

Figure 9 Boiled EGG Model for L0, L1, L2 & L3

The Boiled EGG Model given in Fig. 9 supports physicochemical results as the point for the standard lies in the outside region. This is an indication that L0 is neither BBB+ nor does it demonstrate good GI absorption. The yolk region gives us information about the ability to cross the BBB, the egg white region points to good GI absorption for drugs that are administered orally (76). These results are in good compliance with the ones tabulated in Table 3. Hence, unlike L0, they can pass through BBB, which is a very selective membrane. This is understood by the presence of their points in the yolk region of the Boiled EGG Model.

3.4.6. Excretion

Drug clearance can help determine the frequency of dosing (77–79). It is expressed in mL per minute per kilogram (mL/min/kg). L1 and L3 show moderate clearance, whereas L0 and L2 demonstrate poor clearance. $T_{1/2}$ provides information about the half-life of the drug. Drugs having small half-lives require more frequent dosing, while those with long half-lives need less frequent dosing (80,81). L0, L1, L2, and L3 all are seen to show ultra-short half-lives, since their values for half-lives are less than 1 hour, which is too small. This necessitates frequent dosages. In cases of NiV infections needing critical care, ultra-short half-lives allow precise control over the drug's effect, minimizing the risk of drug accumulation inside the body. This offers an advantage of safety, because the drug's effects can be stopped immediately if any adverse reactions occur. Drugs with ultrashort half-lives require specialized delivery methods.

3.4.7. Toxicology

L1 is least likely to exhibit neurotoxicity, while L2 is most likely to do so. L1 and L3 are not expected to exhibit neurotoxicity, whereas L0 and L2 might show moderate neurotoxicity because their values lie between 0.3 and 0.7. Neurotoxicity trend: **L1<L3<L0<L2**. L0 might cause damage to the inner ear, either by directly damaging the ear's structure or by affecting the nervous system (82–85). Ototoxicity trend: **L1<L3<L2<L0**. Adverse effects on blood-forming organs are known as hematotoxicity. L0 is most likely to demonstrate hematotoxicity. Hematotoxicity trend: **L2<L3<L0<L1.** L1, followed by L0, are more likely to affect the kidneys and cause nephrotoxicity. L0 can cause toxicity to the genes, potentially leading to cancer, while L2 is the least likely to cause genotoxicity. Genotoxicity trend: **L2<L1<L3<L0**. Results show that L0 has the highest chance of causing immunotoxicity, whereas L1 has the least chance of causing toxicity to the RPMI-8226 cell lines. Immunotoxicology: **L1<L2<L3<L0**. A549 is a human non-small cell lung cancer cell line (86–90). The probability of causing toxicity to this cell line is indicated by the trend **L0<L2<L1<L3**. If hERG is blocked, it might lead to long QT syndrome, arrhythmia, and torsades de pointes (TDP), leading to palpitations

or even sudden death (91–96). None of the ligands are hERG blockers. L0 has the highest probability of inducing liver injury (hepatotoxicity) and exhibiting drug-induced liver injury (DILI), while the three stereoisomers fall within the moderate range, suggesting they do not have issues associated with hepatotoxicity and DILI. The Ames Mutagenicity test is important as it is closely related to carcinogenicity (97–100). The predictions suggest that L0 has the highest probability of causing mutagenicity, while L2 has the least chance of causing carcinogenicity due to mutagenicity. For evaluating safety, acute toxicity in mammals is determined. All ligands show very low toxicity and are all non-carcinogenic. L0 has the least probability of irritating the eye, whereas L1 has the highest. L1 and L2 have values very close to one, which indicates that they can cause respiratory toxicity. On the other hand, L0 and L3 are non-respiratory toxicants. In all the ligands, there are zero alerts for acute toxicity, genotoxic carcinogenicity, non-genotoxic carcinogenicity, and skin sensitization rules, meaning that no studied substructures might cause problems associated with these rules. The standard-L0 has one substructure that is not biodegradable, while the three stereoisomers have two substructures that might result in aquatic toxicity.

4. Conclusion

In this research work, the attachment glycoprotein of Nipah virus has been taken as the druggable target. L1, L2 and L3 showed binding scores of -6.7, -7.5 and -7.8 kcal/mol, respectively, better than the standard-Ribavirin (L0) when docked with the attachment glycoprotein of NiV. All 3 stereoisomers show differences in their properties due to the change in stereochemistry. This shows that stereoisomerism can have a significantly high impact on a molecule's binding energy and ADMET profile. NiV infections rapidly reach the brain, causing inflammation of the brain; hence, an effective drug that can cross the BBB and progress to the CNS is required. Ribavirin has severe toxicity issues, no permeation through the BBB, which is critical for NiV and has poor absorption in the GI tract, limiting its efficacy. L1, L2 and L3 show better properties and the ability to permeate through the BBB, better absorption and reduced toxicity problems. Hence, according to the current study, the 3 stated stereoisomers- (1R,2R,4aS,6S,8aS)-2,5,5,8a-tetramethyl-5'-oxo-octahydro-2H-spiro[naphthalene-1,2'-oxolan]-6-yl acetate, Vitedoin B and (1S,2S,4aR,6R,8aR)-2,5,5,8a-tetramethyl-5'-oxo-octahydro-2H-spiro[naphthalene-1,2'-oxolan]-6-yl acetate can be potent candidates in the novel drug discovery of NiV due to their improved physicochemical and medicinal properties along with considerably better and suitable ADMET profiles in context of NiV as compared to the standard - Ribavirin.

Compliance with ethical standards

Acknowledgments

We acknowledge and are grateful to the Director of The Institute of Science, Mumbai, for the support and recognition. No financial support was received for the authorship or publication of this article.

Disclosure of conflict of interest

All authors certify that they have no affiliations with or involvement in any organization or entity with any financial interest or non-financial interest in the subject matter or materials discussed in this manuscript.

Author's Contributions

KBZS has prepared the original draft, conceptualized and visualized the study, curated the data, performed the necessary methodology and formal data analysis using all the software's, while SPP supervised and guided the whole process along providing critical reviews. DNR not only contributed to formatting and proof reading the document but also helped with troubleshooting of software's.

References

[1] Nath A, Banerjee S, Poddar D, Kumar H, Mukherjee D, Parag Soni N, et al. Understanding the dynamics of nipah virus (NiV) transmission and outbreaks in India from Kerala's perspective. Future Health. 2024 Sept 26;2:158–61.

[2] Dhananjay S, Kumari R, Kumar R. Recent Advancement and Novel Approaches of Nipah Virus: An Overview.

[3] Saha O, Siddiquee NH, Akter R, Sarker N, Bristi UP, Sultana KF, et al. Antiviral Activity, Pharmacoinformatics, Molecular Docking, and Dynamics Studies of Azadirachta indica Against Nipah Virus by Targeting Envelope Glycoprotein: Emerging Strategies for Developing Antiviral Treatment. Bioinforma Biol Insights. 2024 Jan;18:11779322241264145.

[4] Randhawa V, Pathania S, Kumar M. Computational Identification of Potential Multitarget Inhibitors of Nipah Virus by Molecular Docking and Molecular Dynamics. Microorganisms. 2022 June 9;10(6):1181.

[5] Chan XHS, Haeusler IL, Choy BJK, Hassan MZ, Takata J, Hurst TP, et al. Therapeutics for Nipah virus disease: a systematic review to support prioritisation of drug candidates for clinical trials. Lancet Microbe. 2024 Nov;101002.

[6] Paliwal S, Shinu S, Saha R. An emerging zoonotic disease to be concerned about - a review of the nipah virus. J Health Popul Nutr. 2024 Oct 28;43(1):171.

[7] Tigabu B, Rasmussen L, White EL, Tower N, Saeed M, Bukreyev A, et al. A BSL-4 High-Throughput Screen Identifies Sulfonamide Inhibitors of Nipah Virus. ASSAY Drug Dev Technol. 2014 Apr;12(3):155–61.

[8] Halpin K, Hyatt AD, Fogarty R, Middleton D, Bingham J, Epstein JH, et al. Pteropid Bats are Confirmed as the Reservoir Hosts of Henipaviruses: A Comprehensive Experimental Study of Virus Transmission. Am Soc Trop Med Hyg. 2011 Nov 1;85(5):946–51.

[9] Howley PM, Knipe DM, editors. Fields virology. Seventh edition. Philadelphia: Wolters Kluwer; 2021.

[10] Goldsmith CS, Whistler T, Rollin PE, Ksiazek TG, Rota PA, Bellini WJ, et al. Elucidation of Nipah virus morphogenesis and replication using ultrastructural and molecular approaches. Virus Res. 2003 Mar;92(1):89–98.

[11] Tamin A, Harcourt BH, Ksiazek TG, Rollin PE, Bellini WJ, Rota PA. Functional Properties of the Fusion and Attachment Glycoproteins of Nipah Virus. Virology. 2002 Apr;296(1):190–200.

[12] Chattu V, Kumar R, Kumary S, Kajal F, David J. Nipah virus epidemic in southern India and emphasizing "One Health" approach to ensure global health security. J Fam Med Prim Care. 2018;7(2):275.

[13] Chowdhury S, Khan SU, Crameri G, Epstein JH, Broder CC, Islam A, et al. Serological Evidence of Henipavirus Exposure in Cattle, Goats and Pigs in Bangladesh. Geisbert T, editor. PLoS Negl Trop Dis. 2014 Nov 20;8(11):e3302.

[14] Harcourt BH, Tamin A, Ksiazek TG, Rollin PE, Anderson LJ, Bellini WJ, et al. Molecular Characterization of Nipah Virus, a Newly Emergent Paramyxovirus. Virology. 2000 June;271(2):334–49.

[15] Debroy B, De A, Bhattacharya S, Pal K. In silico screening of herbal phytochemicals to develop a Rasayana for immunity against Nipah virus. J Ayurveda Integr Med. 2023 Nov;14(6):100825.

[16] N. Jagtap M, T. Borade P, V. Bodake S, B. Darekar A. Enhancing the science in the Global transmission of Nipah virus. Asian J Pharm Res. 2024 Sept 20;295–302.

[17] Tan FH, Sukri A, Idris N, Ong KC, Schee JP, Tan CT, et al. A systematic review on Nipah virus: global molecular epidemiology and medical countermeasures development. Virus Evol. 2024 Aug 7;10(1):veae048.

[18] Safdar M, Rehman SU, Younus M, Rizwan MA, Kaleem M, Ozaslan M. One Health approach to Nipah virus prevention. Vacunas. 2024 Apr;25(2):264–73.

[19] Domingo-Fernández D, Gadiya Y, Preto AJ, Krettler CA, Mubeen S, Allen A, et al. Natural Products Have Increased Rates of Clinical Trial Success throughout the Drug Development Process. J Nat Prod. 2024 July 26;87(7):1844–51.

[20] Sharma N, Varma V, Verma S. Plant-Derived Compounds for Chemoprevention and Chemotherapy: From Molecular Mechanisms to Clinical Trials. In: George B, editor. Bioactive Compounds from Medicinal Plants for Cancer Therapy and Chemoprevention [Internet]. BENTHAM SCIENCE PUBLISHERS; 2024 [cited 2025 Jan 7]. p. 120–55. Available from: https://www.eurekaselect.com/node/233812

[21] Elbadawi M, Efferth T. In Vivo and Clinical Studies of Natural Products Targeting the Hallmarks of Cancer. In Berlin, Heidelberg: Springer Berlin Heidelberg; 2024 [cited 2025 Jan 7]. (Handbook of Experimental Pharmacology). Available from: https://link.springer.com/10.1007/164_2024_716

[22] Ribeiro-Filho J, Teles YCF, Igoli JO, Capasso R. Editorial: New trends in natural product research for inflammatory and infectious diseases: Volume II. Front Pharmacol. 2023 Jan 26;14:1144074.

[23] Fijałkowski Ł, Skubiszewska M, Grześk G, Koech FK, Nowaczyk A. Acetylsalicylic Acid–Primus Inter Pares in Pharmacology. Molecules. 2022 Dec 1;27(23):8412.

[24] Dasgeb B, Kornreich D, McGuinn K, Okon L, Brownell I, Sackett DL. Colchicine: an ancient drug with novel applications. Br J Dermatol. 2018 Feb;178(2):350–6.

[25] Su H, Yao S, Zhao W, Zhang Y, Liu J, Shao Q, et al. Identification of pyrogallol as a warhead in design of covalent inhibitors for the SARS-CoV-2 3CL protease. Nat Commun. 2021 June 15;12(1):3623.

[26] Xu Z, Eichler B, Klausner EA, Duffy-Matzner J, Zheng W. Lead/Drug Discovery from Natural Resources. Molecules. 2022 Nov 28;27(23):8280.

[27] Du R, Cooper L, Chen Z, Lee H, Rong L, Cui Q. Discovery of chebulagic acid and punicalagin as novel allosteric inhibitors of SARS-CoV-2 3CLpro. Antiviral Res. 2021 June;190:105075.

[28] Ashhurst AS, Tang AH, Fajtová P, Yoon MC, Aggarwal A, Bedding MJ, et al. Potent Anti-SARS-CoV-2 Activity by the Natural Product Gallinamide A and Analogues via Inhibition of Cathepsin L. J Med Chem. 2022 Feb 24;65(4):2956–70.

[29] Otsuki K, Li W, Asada Y, Chen CH, Lee KH, Koike K. Daphneodorins A–C, Anti-HIV Gnidimacrin Related Macrocyclic Daphnane Orthoesters from Daphne odora. Org Lett. 2020 Jan 3;22(1):11–5.

[30] Rahim A, Saito Y, Miyake K, Goto M, Chen CH, Alam G, et al. Kleinhospitine E and Cycloartane Triterpenoids from Kleinhovia hospita. J Nat Prod. 2018 July 27;81(7):1619–27.

[31] Wu H, Ma G, Yang Q, Zhu Y, Huang L, Tian Y, et al. Discovery and synthesis of novel beesioside I derivatives with potent anti-HIV activity. Eur J Med Chem. 2019 Mar;166:159–66.

[32] Jalil B, Rollinger JM, Atanasov AG, Singla RK, Kinghorn AD, Heinrich M. Core publications in drug discovery and natural product research. Front Nat Prod. 2024 Nov 11;3:1493720.

[33] Smyrniotopoulos V, Merten C, Kaiser M, Tasdemir D. Bifurcatriol, a New Antiprotozoal Acyclic Diterpene from the Brown Alga Bifurcaria bifurcata. Mar Drugs. 2017 Aug 2;15(8):245.

[34] Sweeney-Jones A, Gagaring K, Antonova-Koch J, Zhou H, Mojib N, Soapi K, et al. Antimalarial Peptide and Polyketide Natural Products from the Fijian Marine Cyanobacterium Moorea producens. Mar Drugs. 2020 Mar 18;18(3):167.

[35] Meesala S, Gurung P, Karmodiya K, Subrayan P, Watve MG. Isolation and structure elucidation of halymeniaol, a new antimalarial sterol derivative from the red alga Halymenia floresii. J Asian Nat Prod Res. 2018 Apr 3;20(4):391–8.

[36] Cheung-Lee WL, Parry ME, Zong C, Cartagena AJ, Darst SA, Connell ND, et al. Discovery of Ubonodin, an Antimicrobial Lasso Peptide Active against Members of the Burkholderia cepacia Complex. ChemBioChem. 2020 May 4;21(9):1335–40.

[37] Pavlik CM, Wong CYB, Ononye S, Lopez DD, Engene N, McPhail KL, et al. Santacruzamate A, a Potent and Selective Histone Deacetylase Inhibitor from the Panamanian Marine Cyanobacterium cf. Symploca sp. J Nat Prod. 2013 Nov 22;76(11):2026–33.

[38] Mascuch SJ, Boudreau PD, Carland TM, Pierce NT, Olson J, Hensler ME, et al. Marine Natural Product Honaucin A Attenuates Inflammation by Activating the Nrf2-ARE Pathway. J Nat Prod. 2018 Mar 23;81(3):506–14.

[39] Mayr LM, Bojanic D. Novel trends in high-throughput screening. Curr Opin Pharmacol. 2009 Oct;9(5):580–8.

[40] Cox PB, Gupta R. Contemporary Computational Applications and Tools in Drug Discovery. ACS Med Chem Lett. 2022 July 14;13(7):1016–29.

[41] Wildey MJ, Haunso A, Tudor M, Webb M, Connick JH. High-Throughput Screening. In: Annual Reports in Medicinal Chemistry [Internet]. Elsevier; 2017 [cited 2025 Jan 4]. p. 149–95. Available from: https://linkinghub.elsevier.com/retrieve/pii/S0065774317300076

[42] Mayr LM, Fuerst P. The Future of High-Throughput Screening. SLAS Discov. 2008 July;13(6):443–8.

[43] Burley SK, Bhatt R, Bhikadiya C, Bi C, Biester A, Biswas P, et al. Updated resources for exploring experimentally-determined PDB structures and Computed Structure Models at the RCSB Protein Data Bank. Nucleic Acids Res. 2025 Jan 6;53(D1):D564–74.

[44] Zardecki C, Dutta S, Goodsell DS, Lowe R, Voigt M, Burley SK. PDB -101: Educational resources supporting molecular explorations through biology and medicine. Protein Sci. 2022 Jan;31(1):129–40.

[45] Iwasa J, Goodsell DS, Burley SK, Zardecki C. A new chapter for RCSB Protein Data Bank Molecule of the Month in 2025. Struct Dyn. 2025 Mar 1;12(2):021101.

[46] Colovos C, Yeates TO. Verification of protein structures: Patterns of nonbonded atomic interactions. Protein Sci. 1993 Sept;2(9):1511–9.

[47] Bowie JU, Lüthy R, Eisenberg D. A Method to Identify Protein Sequences That Fold into a Known Three-Dimensional Structure. Science. 1991 July 12;253(5016):164–70.

[48] Lüthy R, Bowie JU, Eisenberg D. Assessment of protein models with three-dimensional profiles. Nature. 1992 Mar;356(6364):83–5.

[49] Rutz A, Sorokina M, Galgonek J, Mietchen D, Willighagen E, Gaudry A, et al. The LOTUS initiative for open knowledge management in natural products research. eLife. 2022 May 26;11:e70780.

[50] Fu L, Shi S, Yi J, Wang N, He Y, Wu Z, et al. ADMETlab 3.0: an updated comprehensive online ADMET prediction platform enhanced with broader coverage, improved performance, API functionality and decision support. Nucleic Acids Res. 2024 July 5;52(W1):W422–31.

[51] Laskowski R, De Beer T. Ramachandran Plot. In: Hancock JM, Zvelebil MJ, editors. Dictionary of Bioinformatics and Computational Biology [Internet]. 1st ed. Wiley; 2004 [cited 2025 May 16]. Available from: https://onlinelibrary.wiley.com/doi/10.1002/9780471650126.dob0603.pub2

[52] Zhou AQ, O'Hern CS, Regan L. Revisiting the Ramachandran plot from a new angle. Protein Sci. 2011 July;20(7):1166–71.

[53] Eisenberg D, Bowie JU, Lüthy R, Choe S. Three-dimensional profiles for analysing protein sequence-structure relationships. Faraday Discuss. 1992;(93):25–34.

[54] Singh S, Dash AK. Physical Properties, Their Determination, and Importance in Pharmaceutics. In: Pharmaceutics [Internet]. Elsevier; 2024 [cited 2025 Apr 2]. p. 67–113. Available from: https://linkinghub.elsevier.com/retrieve/pii/B9780323997966000023

[55] Loftsson T. Physicochemical Properties and Pharmacokinetics. In: Essential Pharmacokinetics [Internet]. Elsevier; 2015 [cited 2025 Apr 2]. p. 85–104. Available from: https://linkinghub.elsevier.com/retrieve/pii/B9780128014110000032

[56] Kumar BRP, Soni M, Bhikhalal UB, Kakkot IR, Jagadeesh M, Bommu P, et al. Analysis of physicochemical properties for drugs from nature. Med Chem Res. 2010 Nov;19(8):984–92.

[57] Kengar MD, Howal RS, Aundhakar DB, Nikam AV, Hasabe PS. Physico-chemical Properties of Solid Drugs: A Review. Asian J Pharm Technol. 2019;9(1):53.

[58] Alur H, Jain B, Dey S, Johnston TP, Jasti BR, Mitra AK. Physicochemical Factors Affecting Biological Activity. In: Ghosh TK, Jasti BR, editors. Theory and Practice of Contemporary Pharmaceutics [Internet]. 1st ed. CRC Press; 2021 [cited 2025 Apr 2]. p. 83–136. Available from: https://www.taylorfrancis.com/books/9781134441952/chapters/10.1201/9780203644478-5

[59] Hageman M. Preformulation Designed to Enable Discovery and Assess Developability. Comb Chem High Throughput Screen. 2010 Feb 1;13(2):90–100.

[60] Kerns EH, Di L. Rules for Rapid Property Profiling from Structure. In: Drug-like Properties: Concepts, Structure Design and Methods [Internet]. Elsevier; 2008 [cited 2025 Apr 2]. p. 37–42. Available from: https://linkinghub.elsevier.com/retrieve/pii/B978012369520850005X

[61] Li B, Wang Z, Liu Z, Tao Y, Sha C, He M, et al. DrugMetric: quantitative drug-likeness scoring based on chemical space distance. Brief Bioinform. 2024 May 23;25(4):bbae321.

[62] Guan L, Yang H, Cai Y, Sun L, Di P, Li W, et al. ADMET-score – a comprehensive scoring function for evaluation of chemical drug-likeness. MedChemComm. 2019;10(1):148–57.

[63] Benet LZ. Effect of route of administration and distribution on drug action. J Pharmacokinet Biopharm. 1978 Dec;6(6):559–85.

[64] Alagga AA, Pellegrini MV, Gupta V. Drug Absorption. In: StatPearls [Internet]. Treasure Island (FL): StatPearls Publishing; 2025 [cited 2025 May 16]. Available from: http://www.ncbi.nlm.nih.gov/books/NBK557405/

[65] Bertram-Ralph E, Amare M. Factors affecting drug absorption and distribution. Anaesth Intensive Care Med. 2023 Apr;24(4):221–7.

[66] Bohnert T, Gan LS. Plasma protein binding: From discovery to development. J Pharm Sci. 2013 Sept;102(9):2953–94.

[67] Zou P, Zheng N, Yang Y, Yu LX, Sun D. Prediction of volume of distribution at steady state in humans: comparison of different approaches. Expert Opin Drug Metab Toxicol. 2012 July;8(7):855–72.

[68] Toutain PL, Bousquet-Mélou A. Volumes of distribution. J Vet Pharmacol Ther. 2004 Dec;27(6):441–53.

[69] Bohnert T, Gan LS. Plasma protein binding: From discovery to development. J Pharm Sci. 2013 Sept;102(9):2953–94.

[70] Smith DA, Di L, Kerns EH. The effect of plasma protein binding on in vivo efficacy: misconceptions in drug discovery. Nat Rev Drug Discov. 2010 Dec;9(12):929–39.

[71] Zhao M, Ma J, Li M, Zhang Y, Jiang B, Zhao X, et al. Cytochrome P450 Enzymes and Drug Metabolism in Humans. Int J Mol Sci. 2021 Nov 26;22(23):12808.

[72] Remmer H. The role of the liver in drug metabolism. Am J Med. 1970 Nov;49(5):617–29.

[73] Almazroo OA, Miah MK, Venkataramanan R. Drug Metabolism in the Liver. Clin Liver Dis. 2017 Feb;21(1):1–20.

[74] Sweeney BP, Bromilow J. Liver enzyme induction and inhibition: implications for anaesthesia. Anaesthesia. 2006 Feb;61(2):159–77.

[75] Manikandan P, Nagini S. Cytochrome P450 Structure, Function and Clinical Significance: A Review. Curr Drug Targets [Internet]. 2018 Jan 5 [cited 2025 May 16];19(1). Available from: http://www.eurekaselect.com/149505/article

[76] Daina A, Zoete V. A BOILED-Egg To Predict Gastrointestinal Absorption and Brain Penetration of Small Molecules. ChemMedChem. 2016 June 6;11(11):1117–21.

[77] Smith DA, Beaumont K, Maurer TS, Di L. Clearance in Drug Design: Miniperspective. J Med Chem. 2019 Mar 14;62(5):2245–55.

[78] Horde GW, Gupta V. Drug Clearance. In: StatPearls [Internet]. Treasure Island (FL): StatPearls Publishing; 2025 [cited 2025 May 16]. Available from: http://www.ncbi.nlm.nih.gov/books/NBK557758/

[79] Toutain PL, Bousquet-Mélou A. Plasma clearance. J Vet Pharmacol Ther. 2004 Dec;27(6):415–25.

[80] Katzung BG, editor. Basic & clinical pharmacology. Fourteenth edition. New York: McGraw-Hill; 2018.

[81] Hahn RG, Lyons G. The half-life of infusion fluids: An educational review. Eur J Anaesthesiol. 2016 July;33(7):475–82.

[82] Cannizzaro E, Cannizzaro C, Plescia F, Martines F, Soleo L, Pira E, et al. Exposure to ototoxic agents and hearing loss: A review of current knowledge. Hear Balance Commun. 2014 Dec;12(4):166–75.

[83] Jereczek-Fossa BA, Zarowski A, Milani F, Orecchia R. Radiotherapy-induced ear toxicity. Cancer Treat Rev. 2003 Oct;29(5):417–30.

[84] Rybak LP, Ramkumar V. Ototoxicity. Kidney Int. 2007 Oct;72(8):931–5.

[85] Aran J. Current perspectives on inner ear toxicity. Otolaryngol Neck Surg. 1995 Jan;112(1):133–44.

[86] Koparal AT, Zeytinoglu M. Effects of Carvacrol on a Human Non-Small Cell Lung Cancer (NSCLC) Cell Line, A549. Cytotechnology. 2003 Nov;43(1–3):149–54.

[87] Xie J, Liu J, Liu H, Liang S, Lin M, Gu Y, et al. The antitumor effect of tanshinone IIA on anti-proliferation and decreasing VEGF/VEGFR2 expression on the human non-small cell lung cancer A549 cell line. Acta Pharm Sin B. 2015 Nov;5(6):554–63.

[88] Choi SJ, Oh JM, Choy JH. Toxicological effects of inorganic nanoparticles on human lung cancer A549 cells. J Inorg Biochem. 2009 Mar;103(3):463–71.

[89] Yin X, Zhou J, Jie C, Xing D, Zhang Y. Anticancer activity and mechanism of Scutellaria barbata extract on human lung cancer cell line A549. Life Sci. 2004 Sept;75(18):2233–44.

[90] Foldbjerg R, Dang DA, Autrup H. Cytotoxicity and genotoxicity of silver nanoparticles in the human lung cancer cell line, A549. Arch Toxicol. 2011 July;85(7):743–50.

[91] Witchel HJ. Drug-induced hERG Block and Long QT Syndrome: hERG, drugs, and LQTS. Cardiovasc Ther. 2011 Aug;29(4):251–9.

[92] Brown AM. hERG Block, QT Liability and Sudden Cardiac Death. In: Chadwick DJ, Goode J, editors. Novartis Foundation Symposia [Internet]. 1st ed. Wiley; 2005 [cited 2025 May 16]. p. 118–35. Available from: https://onlinelibrary.wiley.com/doi/10.1002/047002142X.ch10

[93] El-Sherif N, Turitto G. The Long QT Syndrome and Torsade De Pointes. Pacing Clin Electrophysiol. 1999 Jan;22(1):91–110.

[94] Tisdale JE, editor. Torsades de pointes. London, United Kingdom: Academic Press, an imprint of Elsevier; 2022. 360 p.

[95] Shah RR. Drug-Induced QT Interval Prolongation—Regulatory Guidance and Perspectives on hERG Channel Studies. In: Chadwick DJ, Goode J, editors. Novartis Foundation Symposia [Internet]. 1st ed. Wiley; 2005 [cited 2025 May 16]. p. 251–85. Available from: https://onlinelibrary.wiley.com/doi/10.1002/047002142X.ch19

[96] Tamargo J. Drug-Induced Torsade de Pointes: From Molecular Biology to Bedside. Jpn J Pharmacol. 2000;83(1):1–19.

[97] Furuhama A, Sugiyama K ichi, Honma M. Ames mutagenicity of 15 aryl, benzyl, and aliphatic ring N-nitrosamines. Regul Toxicol Pharmacol. 2025 Feb;156:105763.

[98] Thompson L, Evans J, Matthews S. Amesformer: State-of-the-Art Mutagenicity Prediction with Graph Transformers [Internet]. Chemistry; 2024 [cited 2025 May 16]. Available from: https://chemrxiv.org/engage/chemrxiv/article-details/67088b6bcec5d6c142d4098f

[99] Guy RC. Ames test. In: Encyclopedia of Toxicology [Internet]. Elsevier; 2024 [cited 2025 May 16]. p. 377–9. Available from: https://linkinghub.elsevier.com/retrieve/pii/B9780128243152011015

[100] Thompson L, Evans J, Matthews S. Amesformer: a graph transformer neural network for mutagenicity prediction [Internet]. Chemistry; 2024 [cited 2025 May 16]. Available from: https://chemrxiv.org/engage/chemrxiv/article-details/66fd0cd5cec5d6c142e23a70